X-ray spectroscopic study of the electronic structure of $CuCrO_2$

T. Arnold, D. J. Payne, A. Bourlange, J. P. Hu, and R. G. Egdell*
Department of Chemistry, Inorganic Chemistry Laboratory, South Parks Road, Oxford OX1 3QR, United Kingdom

L. F. J. Piper, L. Colakerol, A. De Masi, P.-A. Glans, T. Learmonth, and K. E. Smith
Department of Physics, Boston University, 590 Commonwealth Avenue, Boston, Massachusetts 02215, USA

J. Guo
Advanced Light Source, Lawrence Berkeley National Laboratory, Berkeley, California 94720, USA

D. O. Scanlon, A. Walsh,† B. J. Morgan, and G. W. Watson
School of Chemistry, Trinity College Dublin, Dublin 2, Ireland
(Received 31 October 2008; published 5 February 2009)

The electronic structure of the *p*-type transparent conducting oxide $CuCrO_2$ has been studied by x-ray photoemission, x-ray absorption, and x-ray emission spectroscopies. The upper part of the valence band derives mainly from Cu 3*d* and Cr 3*d* states while the lower valence-band states are of dominant O 2*p* atomic character, but with pronounced mutual hybridization among Cu 3*d*, Cr 3*d*, and O 2*p* states. Site specific electronic excitations have been studied by resonant inelastic x-ray scattering at the Cu *L* and Cr *L* edges. Inelastic loss at the Cu *L* edge is dominated by on-site interband excitations similar to those found in Cu_2O, while at the Cr *L* edge localized excitations arising from ligand field splitting of the Cr 3*d* levels are observed. Mg doping on the Cr sites in $CuCrO_2$ is shown to lead to a pronounced shift in the Fermi level toward the edge of the valence band. The experimental data are compared to electronic structure calculations on $CuCrO_2$ carried out using density-functional methods corrected for onsite Coulomb repulsion.

DOI: 10.1103/PhysRevB.79.075102 PACS number(s): 73.20.At, 73.43.Cd, 78.70.En

I. INTRODUCTION

Transparent conducting oxides (TCOs) are a technologically important class of solid-state material which combine the properties of optical transparency in the visible region with a high electrical conductivity.[1] Simple post-transition metal oxides such as ZnO, In_2O_3, and SnO_2 are wide gap insulators which can be doped *n* type, typically by substitution of the host cation with the element to the right in the periodic table. The charge neutrality level in these oxides lies either within the conduction band itself[2] or close thereto and it is relatively straightforward to produce highly degenerate *n*-type material with carrier concentrations in excess of 10^{21} cm^{-3} in the case of In_2O_3.[3] In contrast *p*-type doping is very difficult[4,5] although there are a handful of reports of successful *p*-type doping in ZnO;[6–8] some based on codoping ZnO with *n*-type donors such as Al, Ga, and In along with an excess of the *p*-type dopant N.[9] In simple chemical terms *p*-type doping involves introduction of holes into the O^{2-} $2p^6$ states from which the top of the valence band is derived, i.e., oxidation of oxide ions. Moreover the topmost valence bands show little dispersion in In_2O_3 and SnO_2 so that even if *p*-type doping is achieved, the hole effective masses must be very high and carrier mobility low.[10–13]

The growing interest in electronic or optoelectronic devices based on transparent *p*-*n* junctions has led to exploration for alternative *p*-type TCOs. To date the most promising materials are Cu(I) oxides. In the parent binary oxide cuprite (Cu_2O) the upper valence-band states are of dominant Cu 3*d* atomic character and introduction of holes involves oxidation of $3d^{10}$ Cu(I) to $3d^9$ Cu(II). This process is chemically tractable and Cu_2O is indeed dopable by native defects to give a *p*-type semiconductor. However, the electronic band gap in Cu_2O is 2.17 eV (Ref. 14) and is therefore too small for application in true TCO devices. The relatively small band gap found for Cu_2O is influenced by the fact that a large Cu 3*d* bandwidth arises from strong Cu-Cu interactions: within the cuprite structure each Cu ion has 12 next-nearest Cu neighbors. It was therefore suggested that larger gaps might be found in ternary Cu(I) oxides with reduced dimensionality in next-nearest-neighbor Cu-Cu interactions. The first of a new family of *p*-type TCOs to exploit this idea was $CuAlO_2$.[15–18] The delafossite structure of this compound[19–21] is shown in Fig. 1. Each Cu atom is linearly coordinated by two oxygen atoms, forming O-Cu-O dumbbells parallel to the *c* axis. The oxygen atoms that terminate the dumbbells are also each coordinated to three Al atoms, oriented such that Al-centered octahedra form AlO_2 layers which lie parallel to the *ab* plane. Two alternative layer stacking sequences are possible to give hexagonal (space group $P6_3/mmc$ with *ABABAB* stacking) (Ref. 19) or rhombohedral (space group $R3$-mh with *ABCABC* stacking) (Ref. 20) polymorphs. The early work on $CuAlO_2$ was followed by study of the closely related oxides $CuGaO_2$ (Refs. 22 and 23) and $CuInO_2$.[24–26] The latter is of particular interest as it is amenable to bipolar doping.[27] The band gap of $CuAlO_2$ was originally reported to be 3.5 eV.[15,16] Most surprisingly the measured optical gaps for the $CuMO_2$ delafossites discussed above were found to follow the order $CuAlO_2$(3.5 eV)$<$$CuGaO_2$(3.6 eV)$<$$CuInO_2$(3.9 eV). Subsequent theoretical work established that delafossites are indeed indirect-gap materials and that both the direct and the lower energy indirect gaps follow the expected sequence $CuAlO_2 > CuGaO_2 > CuInO_2$. The apparently anomalous sequence of optical onset energies arises

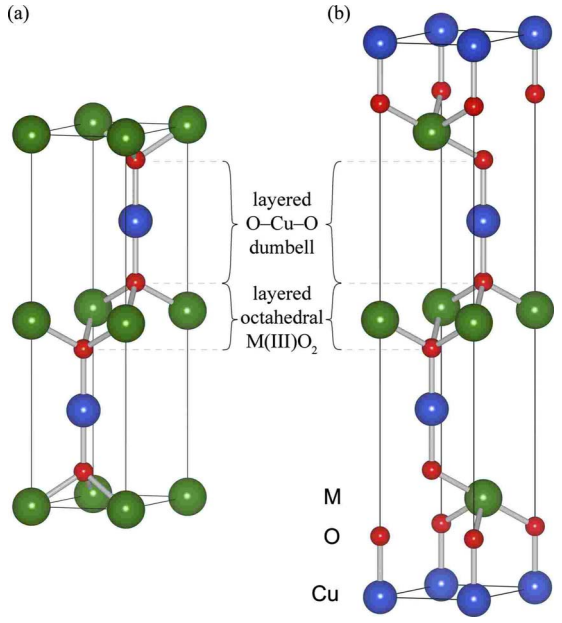

FIG. 1. (Color online) Unit cells for the two polymorphs of the delafossite structure adopted by $CuAlO_2$ and $CuCrO_2$. (a) 2*H* structure; (b) 3*R* structure.

from very low dipole intensity in the absorption spectrum even above the direct threshold for $CuInO_2$.[27] The actual magnitude of the indirect gap in $CuAlO_2$ remains controversial. The experimental value of 1.8 eV which was suggested by Yanagi *et al.*[16] has been called into question on the basis of calculations using a hybrid Hartree-Fock density-functional Hamiltonian. These calculations are expected to give reasonable estimates of absolute values of bulk band gaps[28] and suggest an indirect gap of 3.9 eV for $CuAlO_2$.[29] However, this value is in turn probably too high.

$CuCrO_2$ has been the focus of recent interest as a further *p*-type TCO. It remains tolerably transparent in the visible region despite the fact that there must be dipole forbidden $3d \rightarrow 3d$ excitations centered on Cr in the visible region. Hole mobilities of 11 $cm^2\ V^{-1}\ s^{-1}$ have been measured with carrier concentrations around 4.75×10^{17} cm^{-3} in thin-film material doped by native defects.[30] Higher levels of *p*-type doping can be achieved by substitution of Cr^{3+} with divalent cations. Mg-doped $CuCrO_2$ has the highest reported *p*-type conduction of any TCO.[31] Other divalent dopants such as Ca,[32] Ni,[33] and Cd (Ref. 34) have also been studied. The onset of strong optical absorption in $CuCrO_2$ occurs at around 3 eV.[34–36] Early photoelectrochemical experiments suggested that the onset was associated with an indirect gap of 3.08 eV (Ref. 35) but more recent absorption measurements are consistent with a direct gap of 3.10 eV.[31] Lower energy indirect gaps of 1.28 eV (Ref. 33) and 1.45 eV (Ref. 30) have also been implicated. Recent theoretical work showed that as with the other delafossites the lowest energy band gap in 2H-$CuCrO_2$ is indeed indirect but that the separation between the lowest energy direct and indirect gaps is only about 0.5 eV.[37] Taking this number in conjunction with the experimental direct gap of 3.1 eV gives an estimate of 2.6 eV for the lowest energy indirect gap.

In the present paper we present a comprehensive study of the electronic structure of $CuCrO_2$ using x-ray photoemission, x-ray absorption, and x-ray emission spectroscopies as probes of partial densities of states. The results are compared to band-structure calculations on $CuCrO_2$.[37] $CuCrO_2$ is of particular interest in the context of resonant inelastic x-ray scattering because of the presence of two different transition metals with widely separated *L* edges. We find that distinct electronic excitations may be accessed by studying x-ray scattering at the Cu *L* and Cr *L* edges.

II. EXPERIMENT

Ceramic samples of $CuCrO_2$ and $CuCr_{0.98}Mg_{0.02}O_2$ were prepared by solid-state reaction between CuO, Cr_2O_3, and (for the doped sample) MgO.[31] The oxides were ground in an agate mortar and pestle, pressed into pellets with tungsten carbide dies, and sintered at 1200 °C for 48 h with intermediate regrinding and pelletization. The pellets were finally quenched into liquid nitrogen to give a phase pure materials whose x-ray diffraction patterns measured in a θ-2θ diffractometer contained only peaks associated with the rhombohedral *R*3 phase. Sample conductivity was measured over a temperature range between 300 and 200 K using a four-probe technique on rectangular bars cut from the pellets. The activation energy for conduction was found to be 0.29 eV for the nominally undoped sample and 0.04 eV for the 2% Mg-doped sample.

High-resolution x-ray photoemission spectra were measured in a Scienta ESCA 300 spectrometer. This incorporates a rotating anode Al $K\alpha$ ($h\nu$=1486.6 eV) x-ray source, a seven-crystal x-ray monochromator, and a 300 mm mean radius spherical sector electron energy analyzer with parallel electron detection system. The x-ray source was ran with 200 mA emission current and 14 kV anode bias, while the analyzer operated at 150 eV pass energy. Gaussian convolution of the analyzer resolution with a linewidth of 260 meV for the x-ray source gives an effective instrument resolution of 450 meV. Samples were cleaned *in situ* by annealing at 400 °C. The C 1*s* to O 1*s* intensity ratio was reduced to below 1/100. Binding energies are referenced to the Fermi energy of a silver sample regularly used to calibrate the spectrometer.

X-ray absorption and emission spectra were measured on two beam lines. Initial measurements on the Cu *L* and O *K* edges were performed on beam line 7.0.1 at the Advanced Light Source (ALS), Lawrence Berkeley National Laboratory. This beam line is equipped with a spherical grating monochromator.[38] Emission spectra were recorded using a Nordgren-type grazing-incidence spherical grating spectrometer.[39] For resonant emission experiments, the beam line was set to have an energy resolution of 500 meV at the O *K* edge and 1 eV at the Cu L_3 edge, and the emission spectrometer was set to have a resolution of 350 meV for O *K* and 750 meV for Cu L_3 edge spectra. Absorption spectra were measured in total fluorescence yield (TFY) and total electron yield (TEY) modes, although only TEY spectra are presented. For the absorption measurements, the beam line resolution was set to 200 meV for the O *K* edge and to 1 eV for the Cu L_3 edge. The absorption spectra were normalized to a reference current from a clean gold mesh positioned in

the path of the photon beam. The energy scales of the O *K* absorption spectra were calibrated relative to the O *K* absorption spectrum of NiO and the Cu *L* emission spectra were calibrated relative to the *L* absorption spectrum of Cu metal. The O *K* emission spectra were calibrated to Zn $L\alpha_{1,2}$ and $L\beta_1$ emission lines of Zn metal in second order, and the Cu *L*-edge emission spectra were calibrated relative to metallic Cu $L\alpha_{1,2}$ and $L\beta_1$ emission spectra measured in first order. The consistency of the calibrations in x-ray photoemission spectroscopy (XPS) and x-ray emission spectroscopy (XES) to within 0.2 eV is demonstrated by the fact that the peak maximum in nonresonant Cu L_3 XES (corresponding to the position of the peak maximum in the Cu 3*d* partial density of states relative to the Cu $2p_{3/2}$ core hole) is at 929.45 eV $\pm$ 0.2 eV while the separation between the Cu $2p_{3/2}$ core level and valence-band peak maxima (the latter again corresponding to the position of the peak maximum in the Cu 3*d* partial density of states) in XPS is 929.65 eV $\pm$ 0.1 eV for $CuCrO_2$.

Further experiments at the O *K* edge and Cr *L* edge were performed at the soft x-ray undulator beam line X1B at the National Synchrotron Light Source (NSLS), Brookhaven National Laboratory, which is also equipped with aspherical grating monochromator and Nordgren-type grazing-incidence spherical grating spectrometer. In the resonant mode, the beam line was set to energy resolutions of 700 meV for the O *K* edge and 1.1 eV for the Cr *L* edge, and the emission spectrometer was set to a resolution of 370 meV for the O *K* edge and 600 meV for the Cr *L* edge. X-ray absorption spectroscopy (XAS) spectra were recorded in TEY mode by measuring the sample drain current and were normalized to the current from a reference Au coated mesh in the incident photon beam. The energy resolution was set at 190 meV for the O *K* edge and 220 meV for the Cr *L* edge. The energy scale of the XAS measurements was calibrated using first and second-order diffraction Ti *L* edge absorption features of rutile TiO_2.

III. RESULTS AND DISCUSSION

A. X-ray photoemission and nonresonant x-ray emission spectra

The experimental valence-band Al $K\alpha$ x-ray photoelectron spectrum of $CuCrO_2$ is shown in Fig. 2 along with O *K* and Cu L_3 x-ray emission spectra excited under nonresonant conditions with photons whose energies were well above the relevant core thresholds. For comparison with the experimental data we repeated the band-structure calculations we have recently performed on 2*H*-$CuCrO_2$ for the 3*R*-$CuCrO_2$ polymorph. Full details of the computational approach that was adopted are given in Ref. 37. In outline, the calculations were performed using density-functional theory (DFT) as embodied in the VASP code. The generalized gradient approximation (GGA) was used with correction for on-site Coulomb interactions (the so-called GGA+*U* method). The Coulomb parameter *U* was assigned a value of 5.2 eV for Cu 3*d* states and 4.0 eV for Cr 3*d* states. These values are selected to give good agreement with valence-band photoemission spectra of Cu_2O and Cr_2O_3, respectively.[37] The

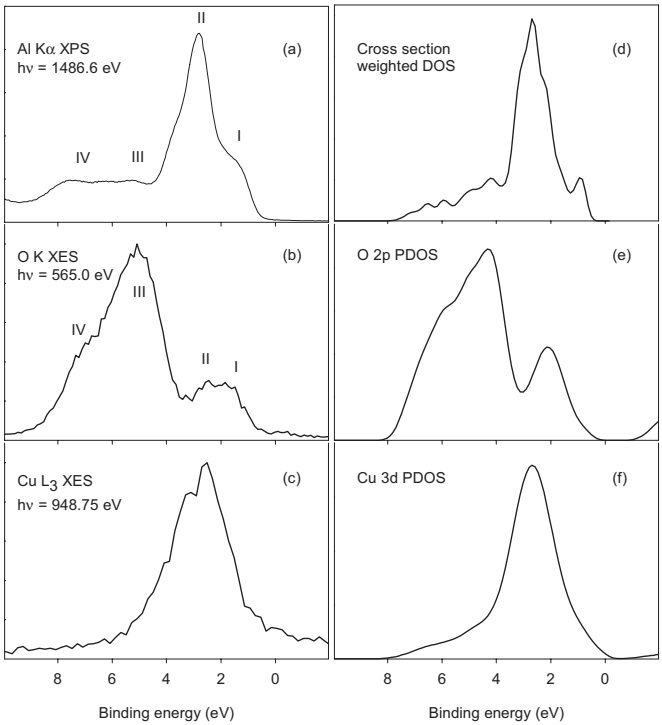

FIG. 2. Left hand panels: (a) Al $K\alpha$ excited valence-band x-ray photoemission, (b) O *K* x-ray emission, and (c) nonresonant Cu L_3 spectra of $CuCrO_2$. The x-ray emission spectra have been shifted to align with the Al $K\alpha$ XPS and are presented on a binding-energy scale. Right hand panels: (d) cross-section-weighted calculated density of states broadened by 0.35 eV, (e) calculated O 2*p* partial density of states broadened by 0.6 eV, and (f) calculated Cu 3*d* partial density of states broadened by 1.2 eV for $CuCrO_2$. The Fermi level has been shifted to above the valence-band edge in order to coincide with the experimental onset energy.

ground state to emerge from these calculations involves antiferromagnetic ordering of spins on the Cr(III) sites along the *c* axis so for the 3*R* polymorph it was necessary to use a $1\times1\times2$ supercell. As expected, the calculated densities of states and bond lengths were virtually identical for 2*H* and 3*R* polymorphs.

The XPS data are compared with the cross-section-weighted density of states, while O *K* and Cu L_3 emission spectra are compared with O 2*p* and Cu 3*d* partial densities of states respectively. Four features labeled I-IV may be identified in the experimental spectra. Reference to the band structure calculations shows that I and II relate to states of dominant Cu 3*d* atomic character while III and IV are associated with states of dominant O 2*p* character. In x-ray photoemission band II is the strongest component of the experimental valence-band spectrum and I appears as an ill resolved shoulder to low binding energy. Bands III and IV are found at higher binding energy and are also weaker than I but of comparable intensity to each other. The one-electron cross section for ionization of Cu 3*d* states is a factor of 20 bigger than for O 2*p* states under Al $K\alpha$ excitation[40] so that the experimental spectrum is dominated by the Cu 3*d* partial density of states even for bands III and IV. In O *K* shell x-ray emission the intensity distribution is reversed and I and II are

much weaker than III and IV. There are also changes of relative intensity within the pairs I, II and III, IV. Specifically II loses intensity relative to I and IV relative to II. The fact that bands I and II appear at all in O *K* shell x-ray emission is a direct consequence of hybridization between Cu 3*d* and O 2*p* states which introduces O 2*p* character into states of nominal Cu 3*d* parentage. The hybridization is stronger for the states in band I than states in band II. This is largely a consequence of the local linear coordination of Cu. Within the linear O-Cu-O units the Cu $3d_z^2$ orbitals have σ-like symmetry, the Cu $3d_{xz}$ and $3d_{yz}$ orbitals π-like symmetry, and the Cu $3d_{xy}$ and Cu $3d_{x^2-y^2}$ orbitals δ-like symmetry. No mixing with O 2*p* states is possible for the Cu 3*d* orbitals of δ symmetry, while the mixing for the π states is weaker than for σ states.[38–41] The observed intensity changes are therefore consistent with the fact that the states in band I are σ-like whereas the δ and π Cu 3*d* states contribute most strongly to band II.

Comparison between Al $K\alpha$ x-ray photoemission spectra of $CuAlO_2$ (Ref. 41) and $CuCrO_2$ [Fig. 3(a)] superficially suggests that Cr 3*d* states are located in the upper part of the valence band between bands I and II, filling in the distinct dip between the two that is found in valence-band XPS of $CuAlO_2$. However, the one-electron cross section for ionization of Cr 3*d* states is only 0.18 kB, whereas the cross section for Cu 3*d* states is 1.2 kB.[40] In addition the nominal electron count is only three for Cr as compared to ten for Cu. As shown in Fig. 3(b) the cross-section-weighted contribution of the Cr 3*d* partial density of states to the Al $K\alpha$ photoemission spectrum is negligible compared to the Cu 3*d* contribution. The differences in the photoemission spectra between $CuAlO_2$ and $CuCrO_2$ may instead be traced to changes in the Cu 3*d* partial density of states when Al is replaced by Cr. In particular replacement of Al by Cr adds spectral weight to the upper part of the valence band. This is apparently via indirect interactions mediated by O, which interacts strongly with both Cu and Cr. It is also noticeable in the experimental spectra that the O 2*p* part of the valence band is broader for $CuAlO_2$ than $CuCrO_2$. Finally replacement of Al by Cr results in pronounced changes in the region of valence-band satellites. For $CuAlO_2$ a single weak satellite labeled s1 in Fig. 3(c) is observed at a binding energy of 16 eV. This is at a similar energy to the satellite in valence region photoemission spectra of Cu_2O which are associated with Cu $3d^8 4(sp)^1$ final states, where $4(sp)^1$ represents excitation of a valence electron into the conduction band.[42,43] The s1 satellite is also present in the photoemission spectrum of $CuCrO_2$, but a second satellite labeled s2 in Fig. 3(d) is observed at a binding energy of just over 10 eV. This corresponds to the valence-band satellite in the photoemission spectrum of Cr_2O_3 associated with an unscreened $3d^2$ final state.[44,45]

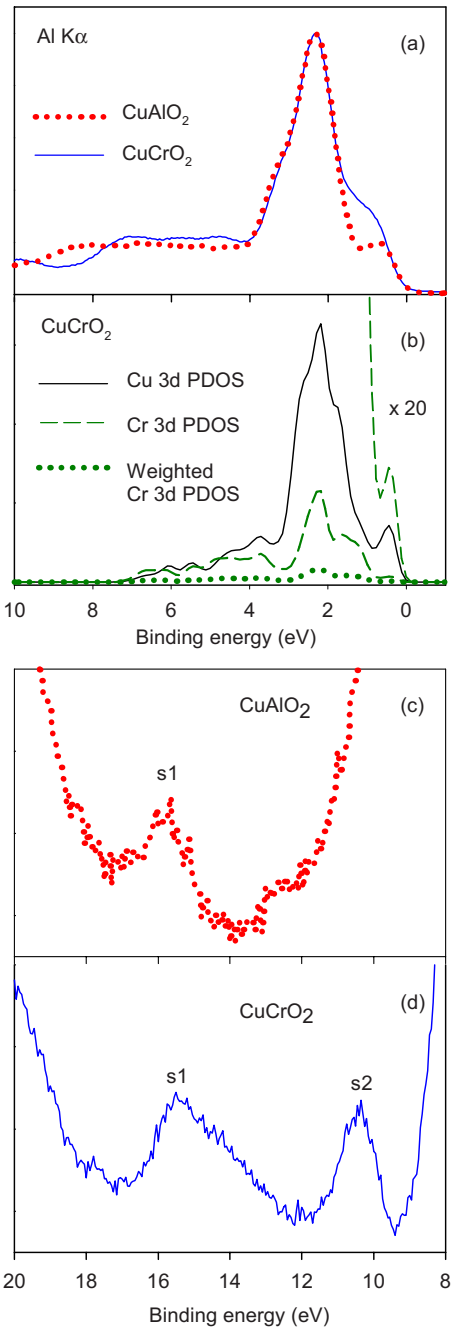

FIG. 3. (Color online) (a) Valence-band Al $K\alpha$ XPS of $CuCrO_2$ compared to that of $CuAlO_2$. The spectra have been subject to small shifts so that the zero in the binding-energy scale coincides with the top of the valence band. (b) Cu 3*d* and Cr 3*d* calculated partial densities of states for $CuCrO_2$, also showing the weighted partial density of states for the Cr 3*d* states obtained by multiplying the raw partial density of states (PDOS) by $\sigma(\text{Cr } 3d)/\sigma(\text{Cu } 3d)$, where σ are one-electron ionization cross sections. (c) Valence satellite region in Al $K\alpha$ XPS of $CuAlO_2$. (d) Valence satellite region in Al $K\alpha$ XPS of $CuCrO_2$.

B. Resonant x-ray scattering and emission at the Cu *L* edge

The x-ray absorption spectrum of $CuCrO_2$ at the Cu L_3 edge is shown in Fig. 4(a). The spectrum is dominated by a sharp peak with a maximum at 934.25 eV, although this is preceded by a very weak prepeak labeled p in the figure. The prepeak is associated with Cu^{2+} $3d^9$ states, i.e., holes in the Cu 3*d* valence band.[41] The position of the bottom of the conduction band is shown as a vertical dashed line in this figure. The placement of this threshold is derived from the measured binding energy of 932.45 eV for the Cu $2p_{3/2}$ core

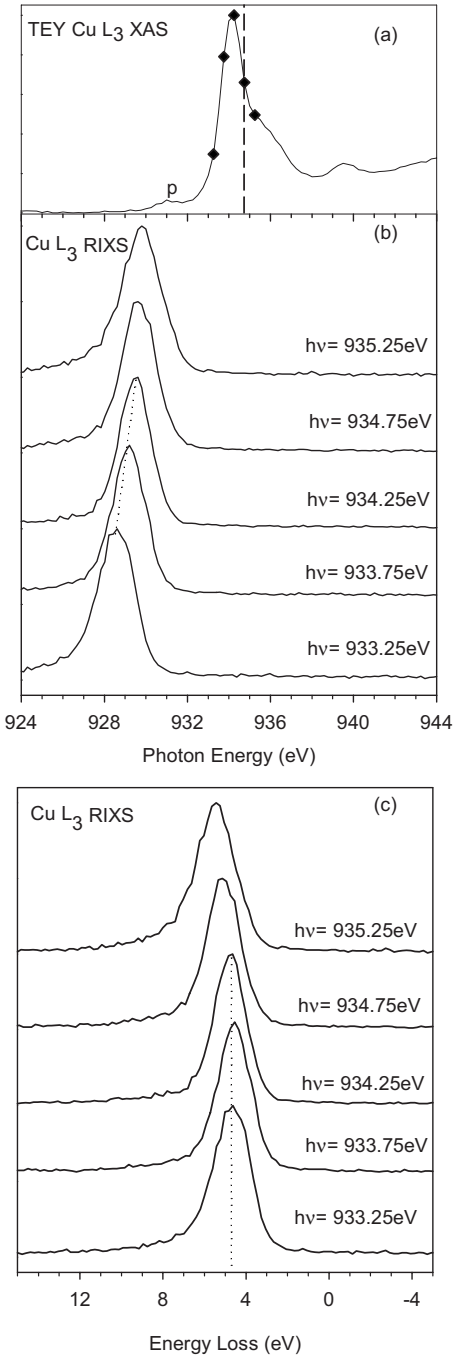

FIG. 4. (a) Total electron yield Cu L_3 x-ray absorption spectrum of $CuCrO_2$. The vertical dashed line shows the location of the bottom of the conduction band derived from analysis of XPS data. The diamonds show the energies used for excitation of x-ray emission spectra. (b) Cu L_3 x-ray emission spectra excited at the emission energies indicated. The prominent emission feature is seen to shift with photon energy for the three lowest excitation energies. (c) Data as in (b) above but plotted on an energy-loss scale. This allows identification of a loss feature at a constant energy of 4.5 eV for the three lowest exciting photon energies.

level in XPS. Assuming that the Fermi level is 0.29 eV above the valence-band maximum, as implied by the measured activation energy for conduction, this fixes the edge of the valence band (932.45 eV−0.29 eV)=932.16 eV above the Cu $2p_{3/2}$ core level. This value must be corrected for the estimated band gap of 2.6 eV for $CuCrO_2$ to give a placement of the bottom of the conduction band (932.16 eV +2.6 eV)=934.76 eV above the Cu $2p_{3/2}$ core level. The peak maximum in the absorption spectrum is seen to lie below the estimated position of the bottom of the conduction band. This implies that the absorption onset is dominated by a strong Coulomb attraction between the excited electron and the core hole to give a core-hole exciton. Very similar behavior has recently been seen for Cu_2O.[46]

Emission spectra excited over a range of photon energies between 933.25 and 935.25 eV are shown in Fig. 4(b). A single broad emission feature is observed which moves to higher energy with increasing exciting photon energy for the three lowest excitation energies. These spectra are transposed onto an energy-loss scale in Fig. 4(c). It is now apparent that the movement seen in Fig. 4(b) corresponds to a constant energy loss of 4.7 eV ± 0.2 eV. This lost energy is very similar to that for inelastic loss features found at the Cu L_3 edge for Cu_2O (Ref. 46) (where the value is 4.5 eV) and $CuAlO_2$ (Ref. 41) (where the value is 5.4 eV). As in these materials the loss feature is assigned to onsite interband excitations from Cu $3d$ states at the top of the valence band into empty conduction-band states which have both Cu $3d$ and Cu $4s$ characters. Both $3d \rightarrow 4s$ and $3d \rightarrow 3d$ excitations are allowed by the $\Delta l = 0, \pm 2$ selection that governs electronic Raman scattering although the $3d \rightarrow 3d$ channel is likely to dominate the spectra because the matrix elements between core $2p$ states and valence $4s$ states are much smaller than corresponding matrix elements between $2p$ and $3d$ states.[47,48] It is interesting to note that resonant inelastic x-ray scattering is only observed for incident photon energies in the excitonic regime.

C. Resonant x-ray scattering and emission at O *K* and Cr *L* edges

The O K and Cr L edges lie within 60 eV of each other so it is instructive to examine absorption and nonresonant emission spectra which encompass both edges. As shown in Fig. 5 Cr L absorption is much stronger than O K absorption but Cr L shell x-ray emission is much weaker than O K emission under nonresonant condition with excitation at $h\nu = 611$ eV. This is attributed to the fact that the fluorescence yield in Cr L shell decay is much lower than the corresponding yield for O K shell decay due to the relatively higher efficiency of Auger decay processes. For this reason it was difficult to gather Cr L emission data with good signal-to-noise ratio.

The O K absorption spectrum is shown in greater detail in Fig. 6(a). As in Fig. 4 the position of the bottom of the conduction band relative to the peak maximum in the O $1s$ core level as estimated from the O $1s$ core-level binding energy is also shown in the figure. In contrast to the Cu L absorption spectrum the peak maximum in the O K absorption spectrum does not lie below the conduction-band minimum, i.e., there is no indication of formation of a true core-hole exciton. However, comparison between the experimental absorption spectrum and the calculated empty O $2p$ partial density of states shows that the distinct peak at

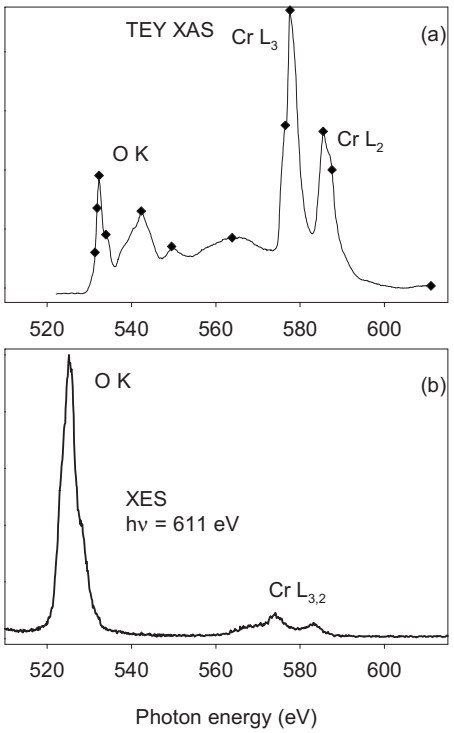

FIG. 5. (a) X-ray absorption spectra of $CuCrO_2$ across the O *K* and Cr *L* edges measured in the total electron yield mode. (b) O *K* and Cr *L* emission spectra measured under excitation by photons with $h\nu$=611 eV.

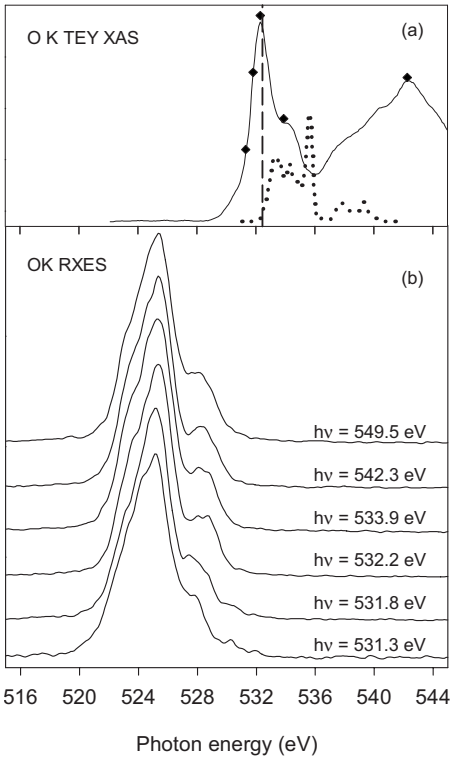

FIG. 6. (a) O *K* x-ray absorption spectrum of $CuCrO_2$ measured in total electron yield mode. The dashed vertical line shows the position of the bottom of the conduction band derived from analysis of XPS data while the diamond shows the energies used for excitation of x-ray emission spectra. The dotted line shows the computed empty O 2*p* partial density of states shifted so that the bottom of the conduction band coincides with the position inferred from XPS. (b) O *K* x-ray emission spectra excited at the photon energies indicated.

the threshold is not a simple feature of the density of states. It therefore appears that the core-hole potential has a strong effect on the absorption spectrum leading to a resonance embedded in the bottom of the conduction band.

Resonant O *K* x-ray emission spectra excited over the range of photon energies close to the O *K* edge threshold highlighted in Fig. 6(a) are shown in Fig. 6(b). Again in contrast to the Cu *L* edge there is no obvious movement in the spectral features with varying photon energy. Thus a simple emission process seems to dominate over resonant inelastic x-ray scattering. This again mirrors results found for $CuAlO_2$ (Ref. 41) and Cu_2O.[46]

The Cr *L* edges present a more complex story. The Cr *L* absorption spectrum is shown in Fig. 7(a). The spectrum is very similar to that of Cr_2O_3 and is dominated by the separation of about 9.5 eV between L_3 and L_2 components with additional fine structure arising from multiplet effects arising from addition of an extra electron to the $3d^3$ configuration. The separation between the Cr L_3 and Cr L_2 onsets is comparable to the width of the valence band. The emission spectra shown in Fig. 7(b) show pronounced shifts in peak positions with exciting photon energy. However, when the spectra are transposed onto an energy-loss scale as in Fig. 7(c) it becomes apparent that a sharp and well-defined loss peak appears at an energy loss of 2.1 eV $\pm$ 0.2 eV. An elastic peak appears as a shoulder on the low energy-loss side of this peak and there are also indications of a broader loss feature at 10 eV, probably associated with charge-transfer excitations The low energy 2.1 eV loss feature arises from ligand field excitations of Cr^{3+}. The Cr^{3+} ion in an octahedral environment has a t_{2g}^3 configuration with a ground state $^4A_{2g}$. The optical-absorption spectrum of Cr_2O_3 and other compounds with Cr^{3+} in an octahedral environment contain two spin-allowed (but dipole forbidden) bands associated with the $^4T_{2g}$ and $^4T_{1g}$ states of the excited $t_{2g}^2 e_g^1$ configuration, as well as spin-forbidden transitions. In electronic Raman scattering, the components of the polarizability tensor span irreducible representations $A_{1g}+E_g+T_{2g}$ so that the transition $^4A_{2g} \rightarrow {}^4T_{1g}$ is allowed but $^4A_{2g} \rightarrow {}^4T_{2g}$ is formally forbidden in a coherent scattering process. The Raman-scattering cross section contains a product of dipole matrix elements connecting initial and final states to a common intermediate state. It might therefore be assumed that since the dipole operator transforms as T_{1u} and the direct product $T_{1u} \times T_{1u} = A_{1g}+E_g+T_{2g}+[T_{1g}]$, transitions mediated by T_{1g} should be allowed. This would include the excitation $^4A_{2g} \rightarrow {}^4T_{2g}$ and indeed Matsubara *et al.*[49] have argued that T_{2g} excited states are accessible. However, $[T_{1g}]$ constitutes the part of the direct product antisymmetric with respect to particle exchange. Owing to the fact that photons are bosons T_{1g} should be excluded in formulation of selection rules. Thus the single observed band is tentatively assigned to the allowed $^4A_{2g} \rightarrow {}^4T_{1g}$ excitation. The corresponding energy of this excitation in Cr_2O_3 is 2.6 eV.[50–52] The lower value for $CuCrO_2$ may reflect reduced Cr-O covalency due to the competition

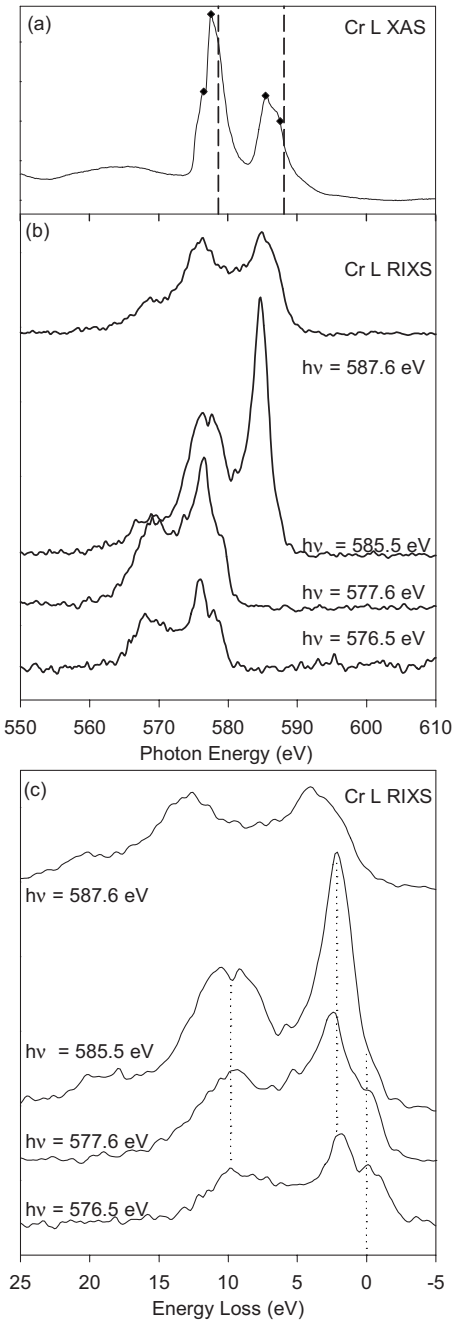

FIG. 7. (a) Cr L x-ray absorption spectrum of $CuCrO_2$ measured in the total electron yield mode. The dashed vertical lines show the position of the bottom of the conduction band derived from analysis of XPS data while the diamonds show the energies used for excitation of x-ray emission spectra. (b) Emission spectra excited at the photon energies indicated. (c) Spectra as in (b) above but plotted on an energy-loss scale. This allows identification of a sharp loss feature at ca. 2.1 eV, together with a broader loss feature at ca. 10 eV.

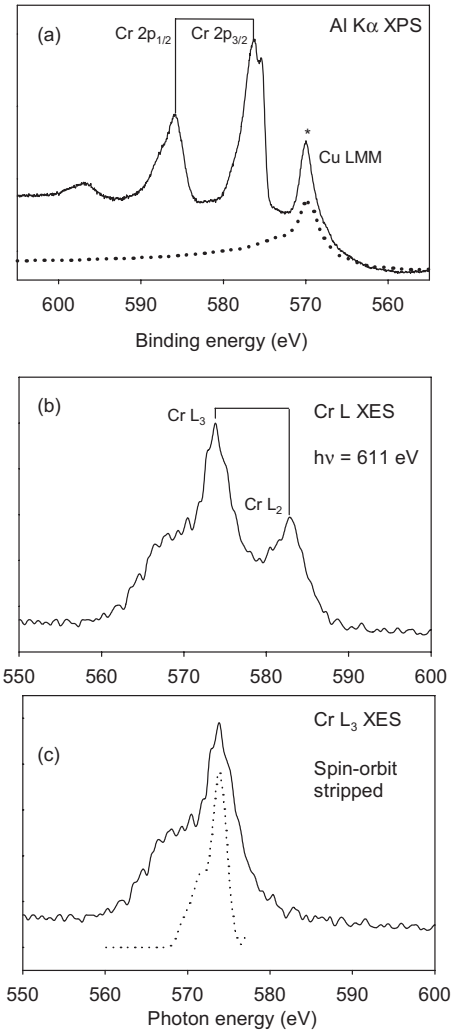

FIG. 8. (a) Cr $2p$ structure in the Al $K\alpha$ X-ray photoelectron spectrum, of $CuCrO_2$. The Cr core lines overlap with Cu LMM Auger structure: the dotted line shows part of the Auger spectrum of Cu_2O. (b) Nonresonant Cr L x-ray emission spectrum of $CuCrO_2$ excited at $h\nu$=611 eV showing L_3 and L_2 components. (c) Solid line: L_3 emission spectrum following spin-orbit stripping of the spectrum in (b) assuming a spin-orbit coupling constant of 9.7 eV. Dotted line: calculated Cr $3d$ partial density of states in $CuCrO_2$ broadened by 1.5 eV.

from formation of short and strong Cu-O bonds. The energy-loss spectra for $CuCrO_2$ are similar to those of Cr_2O_3 as reported by Matsubara *et al.*[49] who despite their theoretical analysis observed a single $3d \rightarrow 3d$ loss peak. These authors analyzed the loss spectra in terms of a model Hamiltonian with a ligand field splitting parameter $10Dq$=1.3 eV and a Coulomb repulsion parameter between $3d$ electrons U_{dd} =5.5 eV. The value for $10Dq$ is much lower than values around 2.06 eV obtained from optical-absorption measurements on thin Cr_2O_3 films.[50–52]

Comparison between nonresonant Cr L shell x-ray emission is complicated by the close proximity of the Cr $2p_{3/2}$ and Cr $2p_{1/2}$ levels seen in both x-ray absorption and core level x-ray photoemission [Fig. 8(a)]. Using a value for the spin-orbit splitting of the core levels from XPS it is however possible to "spin-orbit strip" the nonresonant Cr L emission spectrum shown in Fig. 8(b) to give the L_3 spectrum. The results of this procedure are shown in Fig. 8(c) along with the broadened Cr $3d$ partial density of states derived from the band-structure calculation. Although the shape of the experimental spectral profile matches that of the computed Cr $3d$ partial density of states the Cr L emission extends

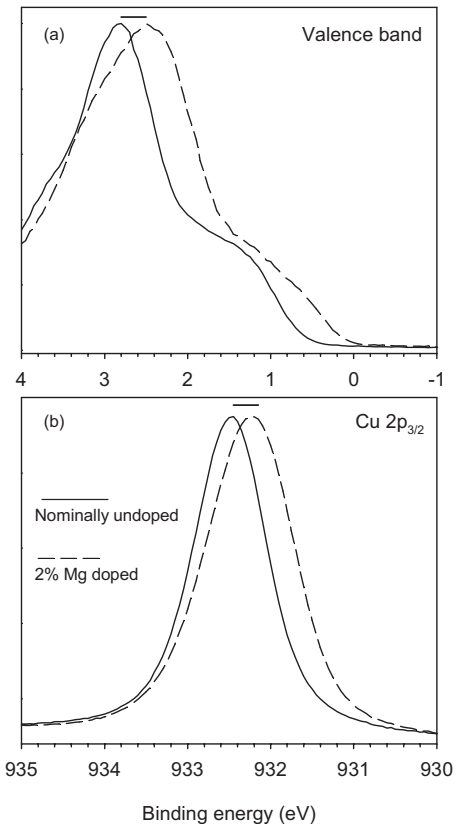

FIG. 9. (a) Valence-band thresholds in Al $K\alpha$ excited valence region photoemission spectra of nominally undoped $CuCrO_2$ and 2% Mg-doped $CuCrO_2$. (b) Cu $2p_{3/2}$ core line in Al $K\alpha$ excited valence region photoemission spectra of nominally undoped $CuCrO_2$ and 2% Mg-doped $CuCrO_2$.

down to lower energy than predicted by the band-structure calculation. This must be due in part to unresolved Cr satellite structure. Although the satellite is relatively weak in Al $K\alpha$ valence-band photoemission, it will have greater relative intensity in Cr L XES, which of course selects out Cr $3d$ spectral weight.

D. Shift in Fermi level with doping

The valence-band photoemission spectrum of $CuCrO_2$ in Fig. 2 showed that the Fermi level in nominally undoped $CuCrO_2$ lays just above the valence-band edge in the lower part of the bulk band gap, as to be expected for a p-type oxide. The valence-band Al $K\alpha$ photoemission onsets for nominally undoped $CuCrO_2$ and 2% Mg-doped $CuCrO_2$ ($CuCr_{0.98}Mg_{0.02}O_2$) are shown in greater detail in Fig. 9(a). There is a well-defined shift to low binding energy with doping, similar to that found for K doping in $SrCu_2O_2$.[53] In nominally undoped $CuCrO_2$ the peak maximum in the valence band is found at 2.80 eV $\pm$ 0.05 eV, while for the Mg doped sample the maximum is at 2.50 eV $\pm$ 0.05 eV. The downward shift of 0.30 eV is therefore close to the change in activation energy for conduction inferred from four-probe conductivity measurements, where a decrease from 0.29 to 0.04 eV (i.e., 0.25 eV) is found. The photoemission measurements therefore confirm that the Fermi level moves toward the valence-band edge with Mg doping. The shift in the valence-band structure is accompanied by corresponding shifts in core level binding energies. Thus Fig. 9(b) shows the Cu $2p_{3/2}$ peaks for nominally undoped and 2% Mg-doped $CuCrO_2$. The peak maximum shifts from 932.45 eV $\pm$ 0.05 eV to 932.20 eV $\pm$ 0.05 eV with Mg doping, again consistent with a change in the activation energy for conduction of 0.25 eV.

IV. CONCLUDING REMARKS

The electronic structure of $CuCrO_2$ has been found to be very similar to that of other Cu(I) oxides where Cu is found in a linear coordination environment. It is difficult to pinpoint the Cr $3d$ states experimentally, but comparison to band-structure calculations suggest that the Cr $3d$ states straddle most of the valence band and hybridize strongly with O $2p$ states at the bottom of the valence band. The significant Cr $3d$ contribution to the top of the valence band suggests that the holes introduced into $CuCrO_2$ by p-type doping are partially delocalized onto Cr. This possibly accounts for the higher conductivity of $CuCrO_2$ as compared with $CuAlO_2$. The presence of two distinct transition-metal ions in this ternary oxide has allowed us to use resonant inelastic x-ray scattering at the two metal L edges to probe site selective electronic excitations. Scattering at the Cu L edge excites onsite interband excitations very similar to those seen in $CuAlO_2$ and Cu_2O, while scattering at the Cr L edge results in excitation of $3d \rightarrow 3d$ transitions arising from ligand field splitting of the Cr $3d$ levels. This selectivity cannot be obtained in conventional optical experiments.

ACKNOWLEDGMENTS

Experimental work on transparent conducting oxides in Oxford is supported under EPSRC Grant No. GR/S94148 and the NCESS Facility by Grant Scienta XPS facility by EPSRC Grant No. EP/E025722/1. The Boston University program is supported in part by the U.S. Department of Energy under Contract No. DE-FG02-98ER45680 and in part by the Donors of the American Chemical Society Petroleum Research Fund. The Advanced Light Source is supported by the Director, Office of Science, Office of Basic Energy Sciences, of the U.S. Department of Energy under Contract No. DE-AC02-05CH11231. Use of the National Synchrotron Light Source, Brookhaven National Laboratory, was supported by the U.S. Department of Energy, Office of Science, Office of Basic Energy Sciences, under Contract No. DE-AC02-98CH10886. The Trinity College Dublin program is funded by Science Foundation Ireland under Grant No. 06/IN.1/I92.

*Corresponding author: russell.egdell@chem.ox.ac.uk
†Present address: National Renewable Energy Laboratory, Golden, Colorado 80401, USA

[1] H. L. Hartnagel, A. L. Dawar, A. K. Jain, and C. Jagadish, *Semiconducting Transparent Thin Films* (IOP, Bristol, 1995).
[2] P. D. C. King, T. D. Veal, D. J. Payne, A. Bourlange, R. G. Egdell, and C. F. McConville Phys. Rev. Lett. **101**, 116808 (2008).
[3] For a discussion of *n*-type doping in In_2O_3, see, e.g., C. G. Granqvist and A. Hultåker, Thin Solid Films **411**, 1 (2002).
[4] A. Tsukazaki, H. Saito, K. Tamura, M. Ohtani, H. Koinuma, M. Sumiya, S. Fuke, T. Fukumura, and M. Kawasaki, Appl. Phys. Lett. **81**, 235 (2002).
[5] S. B. Zhang, S.-H. Wei, and A. Zunger, Phys. Rev. B **63**, 075205 (2001).
[6] T. Yamamoto and H. K. Yoshida, Jpn. J. Appl. Phys., Part 2 **38**, L166 (1999).
[7] M. Joseph, H. Tabata, and T. Kawai, Jpn. J. Appl. Phys., Part 2 **38**, L1205 (1999).
[8] A. Tsukazaki, A. Ohtomo, T. Onuma, M. Ohtani, T. Makino, M. Sumiya, K. Ohtani, S. F. Chichibu, S. Fuke, Y. Segawa, H. Ohno, H. Koinuma and M. Kawasaki, Nature Mater. **4**, 42 (2005).
[9] T. Yamamoto and H. Katayama-Yoshida, Jpn. J. Appl. Phys., Part 2 **38**, L166 (1999).
[10] P. Erhart, A. Klein, R. G. Egdell, and K. Albe, Phys. Rev. B **75**, 153205 (2007).
[11] A. Walsh, J. L. F. Da Silva, S.-H. Wei, C. Körber, A. Klein, L. F. J. Piper, A. DeMasi, K. E. Smith, G. Panaccione, P. Torelli, D. J. Payne, A. Bourlange, and R. G. Egdell, Phys. Rev. Lett. **100**, 167402 (2008).
[12] F. Fuchs and F. Bechstedt, Phys. Rev. B **77**, 155107 (2008).
[13] A. Walsh, J. L. F. Da Silva, and S.-H. Wei, Phys. Rev. B **78**, 075211 (2008).
[14] S. Nikitine, J. B. Grun, and M. Sieskind, J. Phys. Chem. Solids **17**, 292 (1961).
[15] H. Kawazoe, M. Yasukawa, H. Hyodo, M. Kurita, H. M. Yanagi, and H. Hosono, Nature **389**, 939 (1997).
[16] H. Yanagi, S. Inoue, K. Ueda, H. Kawazoe, H. Hosono, and N. Hamada, J. Appl. Phys. **88**, 4159 (2000).
[17] H. Katayama-Yoshida, K. Sato, H. Kizaki, H. Funashima, I. Hamada, T. Fukushima, V. A. Dinh, and M. Toyoda, Appl. Phys. A **89**, 19 (2007).
[18] I. Hamada and H. Katayama-Yoshida, Physica B **376-377**, 808 (2006).
[19] O. Crottaz and F. Kubel, Z. Kristallogr. **211**, 481 (1966).
[20] O. Crottaz and F. Kubel, Z. Kristallogr. **211**, 482 (1996).
[21] O. Crottaz, F. Kubel, and H. Schmid, J. Solid State Chem. **122**, 247 (1996).
[22] K. Ueda, T. Hase, H. Yanagi, H. Kawazoe, H. Hosono, H. Ohta, M. Orita, and M. Hirano, J. Appl. Phys. **89**, 1790 (2001).
[23] H. Yanagi, H. Kawazoe, A. Kudo, M. Yasukawa, and H. Hosono, J. Electroceram. **4**, 407 (2000).
[24] H. Yanagi, T. Hase, S. Ibuki, K. Ueda, and H. Hosono, Appl. Phys. Lett. **78**, 1583 (2001).
[25] H. Yanagi, K. Veda, H. Ohta, M. Orita, M. Hirano, and H. Hosono, Solid State Commun. **121**, 15 (2001).
[26] L. Liu, K. Bai, H. Gong, and P. Wu, Phys. Rev. B **72**, 125204 (2005).
[27] X. L. Nie, S.-H. Wei, and S. B. Zhang, Phys. Rev. Lett. **88**, 066405 (2002).
[28] J. Muscat, A. Wander, and N. M. Harrison, Chem. Phys. Lett. **342**, 397 (2001).
[29] J. Robertson, P. Peacock, M. Towler, and R. Needs, Thin Solid Films **411**, 96 (2002).
[30] S. Mahapatra and S. Shivashankar, Chem. Vap. Deposition **9**, 238 (2003).
[31] R. Nagarajan, A. Draeseke, A. Sleight, and J. Tate, J. Appl. Phys. **89**, 8022 (2001).
[32] H. Huang, C. F. Zhu, and W. Liu, Chin. J. Chem. Phys. **17**, 161 (2004).
[33] S. Y. Zheng, G. S. Jiang, J. R. Su, and C. F. Zhan, Mater. Lett. **60**, 3871 (2006).
[34] M. Lalic and J. Mestnik-Filho, J. Phys.: Condens. Matter **18**, 1619 (2006).
[35] F. A. Benko and F. P. Koffyberg, Mater. Res. Bull. **21**, 753 (1986).
[36] D. Li, X. Fang, Z. Deng, S. Zhou, R. Tao, W. Dong, T. Wang, Y. Zhou, G. Meng, and X. Zhu, J. Phys. D **40**, 4910 (2007).
[37] D. O. Scanlon, A. Walsh, B. J. Morgan, G. W. Watson, D. J. Payne, and R. G. Egdell, Phys. Rev. B **79**, 035101 (2009).
[38] J. Nordgren and R. Nyholm, Nucl. Instrum. Methods Phys. Res. A **246**, 242 (1986).
[39] J. Nordgren, G. Bray, S. Cramm, R. Nyholm, J. E. Rubensson, and N. Wassdahl, Rev. Sci. Instrum. **60**, 1690 (1989).
[40] J. J. Yeh and I. Lindau, At. Data Nucl. Data Tables **32**, 1 (1985).
[41] D. J. Aston, D. J. Payne, A. J. H. Green, R. G. Egdell, D. S. L. Law, J. Guo, P. A. Glans, T. Learmonth, and K. E. Smith, Phys. Rev. B **72**, 195115 (2005).
[42] J. Ghijsen, L. H. Tjeng, H. Eskes, G. A. Sawatzky, and R. L. Johnson, Phys. Rev. B **42**, 2268 (1990).
[43] J. P. Hu, D. J. Payne, R. G. Egdell, N. M. Harrison, and V. R. Dhanak, Chem. Phys. Lett. **450**, 39 (2007).
[44] D. E. Eastman and J. L. Freeouf, Phys. Rev. Lett. **34**, 395 (1975).
[45] R. Zimmermann, P. Steiner, and S. Hüfner, J. Electron Spectrosc. Relat. Phenom. **78**, 49 (1996).
[46] J. P. Hu, D. J. Payne, R. G. Egdell, P.-A. Glans, T. Learmonth, K. E. Smith, J. Guo, and N. M. Harrison, Phys. Rev. B **77**, 155115 (2008).
[47] U. Fano and J. W. Cooper, Rev. Mod. Phys. **40**, 441 (1968).
[48] M. Grioni, J. B. Goedkoop, R. Schoorl, F. M. F. deGroot, J. C. Fuggle, F. Schafers, E. E. Koch, G. Rossi, J. M. Esteva, and R. C. Karnatak, Phys. Rev. B **39**, 1541 (1989).
[49] M. Matsubara, T. Uozumi, A. Kotani, Y. Harad, and S. Shin, J. Phys. Soc. Jpn. **71**, 347 (2002).
[50] D. S. McClure, J. Chem. Phys. **38**, 2289 (1963).
[51] C. M. Mo, W. L. Cai, G. Chen, X. M. Li, and L. Zhang, J. Phys.: Condens. Matter **9**, 6103 (1997).
[52] M. G. Brik, N. M. Avram, and C. N. Avram, Solid State Commun. **132**, 831 (2004).
[53] C. C. B. Lynch, R. G. Egdell, and D. S. L. Law, Chem. Phys. Lett. **401**, 223 (2005).